Paper 50

Proceedings of the Eleventh International Conference
on Computational Structures Technology,
B.H.V. Topping, (Editor),
Civil-Comp Press, Stirlingshire, Scotland

Elastic Solids Reinforced with Random Fibres Developing Large Deformations: A Finite Element Approach

M.S.M. Sampaio, H.B. Coda and R.R. Paccola
São Carlos School of Engineering
University of São Paulo, Brazil

Abstract

This paper is devoted to introduce curved fibre with high order approximations in a continuum media via tailoring process demonstrating that, if the order of fibre approximation is at least the same as the solid finite element, the coupling is conforming and the deficiency of the technique disappears, that is, does not guarantee the continuity among the continuum and the fibre material between nodes. Moreover, the spreading strategy that makes it possible to make a complete analysis of randomly fibre reinforced materials without increasing the number of variables. Applications for two dimensional large deformation analysis of elastic bodies shows the potential of the proposed formulation.

Keywords: finite element method, geometrical non-linearity, fibre-reinforced solids, curved fibre finite elements, tailoring, conform coupling fibre-matrix.

1 Introduction

Fibre reinforced solids are usually analyzed by homogeneous analog which makes difficult to identify the contact stresses between fibres and matrix. Alternatively, interesting techniques proposing the fibre-matrix coupling are present in literature. Some of them introduce fibres into continuum by direct mathematical considerations generating solid finite elements that consider fibres properties [1-3]. Others introduce fibres as a point to point bar discretization which leads to a difficult mesh generation process. Another strategy is to write fibre nodes coordinates as functions of solid finite elements nodes by means of shape functions and introduce the strain energy of fibres into the solution process [4].

The last strategy makes possible to consider fibres at any place of the continuum without increasing the amount of unknowns in the solution procedure. However, in general, it does not guaranty the continuity among the continuum and fibre material between nodes and, as a consequence, this technique is called tailoring process [1].

In this paper we develop a curved fibre finite element with high order approximations based on tailoring description that ensures the conform coupling between fibre-matrix. The nodal parameters are positions, not displacements. The formulation is classified as total Lagrangian and the Saint-Venant-Kirchhoff constitutive law [5, 6] is chosen to model the material behavior.

To solve geometrical nonlinear problems we adopt the Principle of Minimum Total Potential Energy [7] and the Newton-Raphson iterative procedure [8] to solve the nonlinear system.

The paper is organized as follows. Section 2 describes the general nonlinear solution process. Section 3 describes the procedure used to model the two-dimensional continuum, plate element. Section 4 presents the any order fibre finite elements and the spreading strategy that makes possible a complete analysis of any order fibres into high order plate finite elements without increasing the number of degrees of freedom. Section 5 presents the numerical examples validating the proposed formulation. Finally, conclusions are presented in Section 6.

2 The non-linear solution

In this section, the strategy adopted to solve the reinforced plate geometrically nonlinear equilibrium is described.

The non-linear analysis starts writing the total potential energy as follows:

$$\Pi(Y) = U(Y) - \Omega(Y) \tag{1}$$

where Π is the total potential energy of the system, U is the strain energy including matrix and fibre contributions written regarding plate nodal positions and Ω is the potential energy of external conservative applied forces given by:

$$\Omega = F_j Y_j \tag{2}$$

where F_j is the vector of external forces and Y_j is the current position vector.

The Principle of Minimum Total Potential Energy [7] is applied writing the equilibrium equation as the derivative of total energy regarding nodal positions (plate for instance), as:

$$g_j = \frac{\partial \Pi}{\partial Y_j} = \frac{\partial U}{\partial Y_j} - F_j = F_j^{int} - F_j = 0 \tag{3}$$

where F_j^{int} is the internal force vector or strain energy gradient vector calculated regarding plate nodal positions. The nodal current positions are the unknowns of the problem, so, when adopting a trial position in Equation (3), g_j is not null and becomes the unbalanced force vector of the Newton-Raphson [8] strategy for

solving nonlinear systems. Expanding the unbalanced force vector around the trial solution Y_l^0, one has:

$$g_j(Y_l) = g_j(Y_l^0) + \left.\frac{\partial g_j}{\partial Y_k}\right|_{(Y_l^0)} \Delta Y_k + O_j^2 = 0 \tag{4}$$

which can be rewritten, neglecting higher order terms as:

$$\Delta Y_k = -\left.\frac{\partial g_j}{\partial Y_k}\right|_{Y_l^0} g_j(Y_l^0) = -\left.\frac{\partial^2 U}{\partial Y_k \partial Y_j}\right|_{Y_l^0} g_j(Y_l^0) \tag{5}$$

where ΔY_k is the correction of position and $\left.\frac{\partial^2 U}{\partial Y_k \partial Y_j}\right|_{Y_l^0}$ is the Hessian matrix or tangent stiffness matrix.

The trial solution is improved by:

$$Y_l = Y_l^0 + \Delta Y_k \tag{6}$$

until ΔY_k or g_j become sufficiently small [8].

3 Isoparametric plate finite element

In this section the necessary expressions to consider the continuum part of a general composite in the solution process are presented.

3.1 Kinematical approximation and positional mapping

Figure 1 shows the matrix mapping from the initial configuration B_0 to its current configuration B. This mapping is done by means of a dimensionless auxiliary configuration B_1.

The initial configuration B_0 whose points have coordinates x_i is mapped from the dimensionless space B_1 with coordinates ξ_i using shape functions of any order, $\phi_l(\xi_1, \xi_2)$, and by the coordinates of the nodes l in the initial configuration, X_i^l, such as:

$$x_i = f_i^0 = \phi_l(\xi_1, \xi_2) X_i^l \tag{7}$$

Similarly, the current configuration B is mapped from the dimensionless space B_1 by the expression:

$$y_i = f_i^1 = \phi_l\left(\xi_1, \xi_2\right) Y_i^l \tag{8}$$

where y_i are coordinates of points in the current configuration, Y_i^l are the current node positions, $l = 1,...,N$ are nodes and $i = 1,2$ correspond to nodal degrees of freedom.

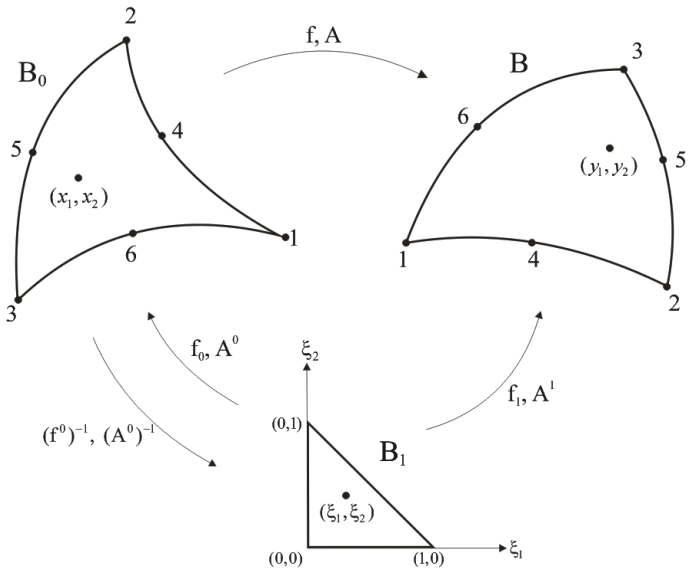

Figure 1: Mapping of the initial and current configurations.

The deformation function $\boldsymbol{f}$ that maps initial configuration B_0 to the current configuration B can be written as a composition of mappings $\boldsymbol{f}^0$ and $\boldsymbol{f}^1$ as:

$$\boldsymbol{f} = \boldsymbol{f}^1 \circ \left(\boldsymbol{f}^0\right)^{-1} \tag{9}$$

The deformation gradient $\boldsymbol{A}$ can be derived directly from $\boldsymbol{A}^0$ and $\boldsymbol{A}^1$ as [9,10]:

$$\boldsymbol{A} = \boldsymbol{A}^1 \cdot (\boldsymbol{A}^0)^{-1}, \text{ with } A_{ij}^0 = \frac{\partial f_i^0}{\partial \xi_j}, \; A_{ij}^1 = \frac{\partial f_i^1}{\partial \xi_j} \tag{10}$$

Equation (10) can be understood as a numerical chain rule because the initial mapping gradient $\boldsymbol{A}^0$ is a known numerical quantity.

3.2 Continuum strain energy

To simulate the continuum portion of the composite (matrix) we adopted the Saint-Venant-Kirchhoff specific strain energy function [5, 6], as:

$$u_{mat} = \frac{1}{2} E_{ij} \mathbb{C}_{ijkl} E_{kl} \tag{11}$$

where $\mathbb{C}_{ijkl}$ is the elastic fourth-order tensor and $\boldsymbol{E}$ is the Green-Lagrange second-order strain expressed respectively by:

$$\mathbb{C}_{ijkl} = \frac{2G\nu}{1-2\nu} \delta_{ij}\delta_{kl} + G\left(\delta_{ik}\delta_{jl} + \delta_{il}\delta_{jk}\right) \tag{12}$$

$$E_{ij} = \frac{1}{2}\left(C_{ij} - \delta_{ij}\right) = \frac{1}{2}\left(A_{ki}A_{kj} - \delta_{ij}\right) \tag{13}$$

The variables $\boldsymbol{C} = \boldsymbol{A}^{\boldsymbol{T}}.\boldsymbol{A}$ and $\boldsymbol{\delta}$ are the right Cauchy-Green stretch tensor and the Kroenecker delta, respectively. In Equation (13), G is the shear modulus and ν is the Poisson's ratio.

The strain energy accumulated in the finite element is calculated by integrating the specific strain energy over the initial volume, i.e.

$$U_{mat} = \int_{V_0} u_{mat} dV_0 \tag{14}$$

Considering plates with unitary thickness and writing Equation (14) as a function of dimensionless coordinates ξ_1 and ξ_2 results:

$$U_{mat} = \int_0^1 \int_0^{1-\xi_2} u_{mat}(\xi_1, \xi_2) J_0(\xi_1, \xi_2) d\xi_1 d\xi_2 \tag{15}$$

where J_0 is the Jacobian of the initial mapping, i.e., $J_0(\xi_1, \xi_2) = det(\boldsymbol{A}^0)$ with $\boldsymbol{A}^0$ given by Equation (10).

If the modelled material has no reinforcement, the strain energy can be derived directly regarding the plate finite element positions finding the conjugate internal forces, as:

$$F_\alpha^{\beta\, int} = \frac{\partial U_{mat}}{\partial Y_\alpha^\beta} = \int_{v_0} \frac{\partial u_{mat}}{\partial Y_\alpha^\beta} dV_0 = \int_0^1 \int_0^{1-\xi_1} \frac{\partial u_{mat}}{\partial Y_\alpha^\beta} J_0(\xi_1, \xi_2) d\xi_2 d\xi_1 \tag{16}$$

The derivative inside the integral term of equation (16) can be developed as:

$$\frac{\partial u_{mat}}{\partial Y_\alpha^\beta} = \frac{\partial u_{mat}}{\partial \boldsymbol{E}} : \frac{\partial \boldsymbol{E}}{\partial \boldsymbol{C}} : \frac{\partial \boldsymbol{C}}{\partial Y_\alpha^\beta} = \frac{1}{2} \boldsymbol{S} : \frac{\partial \boldsymbol{C}}{\partial Y_\alpha^\beta} \tag{17}$$

where $\boldsymbol{S} = \partial u_{mat} / \partial \boldsymbol{E}$ is the second Piola-Kirchhoff stress tensor and $\boldsymbol{C}$ is the right Cauchy-Green stretch tensor.

In the solution process, Section 2, it is necessary to calculate the second derivative of strain energy regarding nodal positions, resulting into the Hessian matrix, that is:

$$H_{\alpha\beta\gamma\xi}^{mat} = \frac{\partial^2 U_{mat}}{\partial Y_\alpha^\beta \partial Y_\gamma^\xi} = \int_{V_0} \frac{\partial^2 u_{mat}}{\partial Y_\alpha^\beta \partial Y_\gamma^\xi} dV_0 \tag{18}$$

in which

$$\frac{\partial^2 u_{mat}}{\partial Y_\alpha^\beta \partial Y_\gamma^\xi} = \frac{1}{4} \frac{\partial^2 u_{mat}}{\partial \boldsymbol{E} \partial \boldsymbol{E}} : \frac{\partial \boldsymbol{C}}{\partial Y_\gamma^\xi} : \frac{\partial \boldsymbol{C}}{\partial Y_\alpha^\beta} + \frac{1}{2} \frac{\partial u_{mat}}{\partial \boldsymbol{E}} : \frac{\partial^2 \boldsymbol{C}}{\partial Y_\gamma^\xi \partial Y_\alpha^\beta} \tag{19}$$

4 Elastic fibre reinforcement – kinematics and energy considerations

This section presents the necessary expressions to introduce the fibres characteristics in the composite formulation.

4.1 Any order curved fibre finite element

Figure 2 shows the non-deformed initial configuration B_0, the current configuration B and a non-dimensional auxiliary configuration B_1 for the curved fibre finite element of any order.

The initial configuration B_0 whose points have coordinates x_i is mapped from the dimensionless space B_1 with coordinates ξ using shape functions of any order, $\phi_P(\xi)$, and by the coordinates of the nodes P in the initial configuration, X_i^P, such as:

$$x_i = f_i^0 = \phi_P(\xi) X_i^P \tag{20}$$

The current configuration B is mapped from the dimensionless space B_1 by the expression

$$y_i = f_i^1 = \phi_P(\xi) Y_i^P \tag{21}$$

where y_i are the coordinates of points in the current configuration B and Y_i^P are the current coordinates of fibre nodes in the current configuration. In Equations (20)-

(21) index $P = 1,...,n$ and $i = 1,2$ represent, respectively, the fibre finite element nodes and the degrees of freedom associated with these nodes.

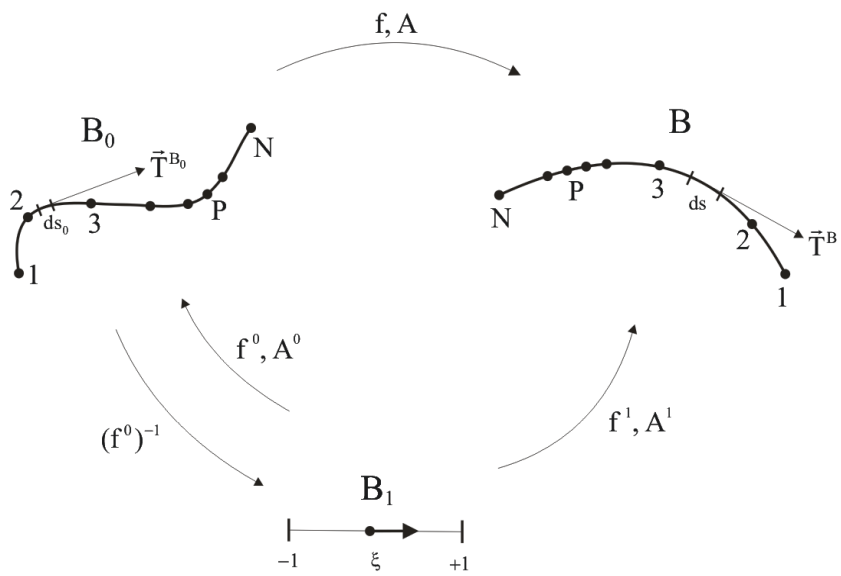

Figure 2: Mapping of the fibre finite element - initial and current configurations.

The tangent vector of the fibre and its modulus are calculated at the initial configuration as:

$$T_i^{B_0} = \frac{d\phi_P(\xi)}{d\xi} X_i^P \text{ and } \left|\vec{T}^{B_0}\right|^2 = \left(\frac{d\phi_P(\xi)}{d\xi} X_1^P\right)^2 + \left(\frac{d\phi_P(\xi)}{d\xi} X_2^P\right)^2 \tag{22}$$

It is important to mention that $\left|\vec{T}_{B^0}\right|$ is the differential Jacobian of f_i^0. For the current configuration one finds:

$$T_i^B = \frac{d\phi_P(\xi)}{d\xi} Y_i^P \text{ and } \left|\vec{T}^B\right|^2 = \left(\frac{d\phi_l(\xi)}{d\xi} Y_1^P\right)^2 + \left(\frac{d\phi_l(\xi)}{d\xi} Y_2^P\right)^2 \tag{23}$$

From the tangent vector modulus, Equations (22)-(23), the one-dimensional Green strain is written as:

$$E = \frac{1}{2}\left(\frac{\left|\vec{T}^B\right|^2 - \left|\vec{T}^{B_0}\right|^2}{\left|\vec{T}^{B_0}\right|^2}\right) \tag{24}$$

which in its expanded form is given by:

$$E=\frac{1}{2}\frac{\left[\left(\frac{d\phi_l(\xi)}{d\xi}Y_1^P\right)^2+\left(\frac{d\phi_l(\xi)}{d\xi}Y_2^P\right)^2\right]-\left[\left(\frac{d\phi_l(\xi)}{d\xi}X_1^P\right)^2+\left(\frac{d\phi_l(\xi)}{d\xi}X_2^P\right)^2\right]}{\left(\frac{d\phi_l(\xi)}{d\xi}X_1^P\right)^2+\left(\frac{d\phi_l(\xi)}{d\xi}X_2^P\right)^2} \quad (25)$$

Using the Saint-Venant-Kirchhoff constitutive law one writes the specific strain energy at a point of the fibre as:

$$u_f(\xi)=\frac{1}{2}\mathbb{E}\left[E(\xi)\right]^2 \quad (26)$$

where $\mathbb{E}$ is the elastic modulus and $E(\xi)$ is the Green strain measure defined in Equations (24) or (25).

The strain energy of a fibre is given by:

$$U_f=\int_{V_0}u_f dV_0 \quad (27)$$

in which V_0 is the initial volume of the fibre element. In order to proceed with the equilibrium analysis it is necessary to know the first derivative of strain energy regarding positions. Based on the energy conjugate concept the natural internal fibre force vector, $F_i^{f\,int}$ is calculated regarding fibre parameters as:

$$F_k^{jf}=\frac{\partial U_f}{\partial Y_k^j}=\int_{V_0}\frac{\partial u_f}{\partial Y_k^j}dV_0 \quad (28)$$

From Equations (25) and (26) follows that

$$F_k^{jf}=\int_0^{L_0}\mathbb{E}E\frac{\left(\frac{d\phi_l(\xi)}{d\xi}Y_k^l\right)\frac{d\phi_j(\xi)}{d\xi}}{\left|T^0\right|^2}Ads_0=\int_{-1}^{1}\mathbb{E}E\frac{\left(\frac{d\phi_l(\xi)}{d\xi}Y_k^l\right)\frac{d\phi_j(\xi)}{d\xi}}{\left|T^0\right|^2}J_0(\xi)Ad\xi \quad (29)$$

where $J_0(\xi)=\left|\vec{T}^0\right|=\sqrt{\left(\frac{dx_1}{d\xi}\right)^2+\left(\frac{dx_2}{d\xi}\right)^2}$.

The Hessian matrix components for the fibre element are obtained by the second derivative of the strain energy, i.e.:

$$H_{kj\alpha\beta}^f=\frac{\partial^2 U_f}{\partial Y_k^j\partial Y_\alpha^\beta}=\int_{V_0^f}\frac{\partial^2 u_f}{\partial Y_k^j\partial Y_\alpha^\beta}dV_0^f \quad (30)$$

Developing the necessary calculations one achieves:

$$H^{f}_{kj\alpha\beta} = \int_{-1}^{1} \left(\frac{\mathbb{E}E}{\left|T^{0}\right|^{4}} \left(\frac{d\phi_l(\xi)}{d\xi} Y^{l}_{\alpha} \right) \frac{d\phi_\beta(\xi)}{d\xi} \left(\frac{d\phi_l(\xi)}{d\xi} Y^{l}_{k} \right) \frac{d\phi_j(\xi)}{d\xi} + \frac{\mathbb{E}E}{\left|T^{0}\right|^{2}} \frac{d\phi_\beta(\xi)}{d\xi} \frac{d\phi_j(\xi)}{d\xi} \delta_{k\alpha} \right) AJ(\xi) d\xi \tag{31}$$

Integrals (29) and (31) are solved using Gauss-Legendre quadrature.

4.2 Kinematical fibre-matrix coupling

The procedure adopted here to place the fibres at any position of the domain without increasing the number of degrees of freedom is based on the work of [4, 11]. These works were concerned with straight linear fibres and triangular plate elements, moreover only linear applications were developed.

The fibre elements are introduced in matrix by means of nodal kinematic relations. In the initial configuration ones written

$$X^{f}_{i} = \phi_l(\xi^{P}_{1}, \xi^{P}_{2}) X^{l}_{i} \tag{32}$$

where ϕ_l are the shape functions of the plate element, X^{P}_{i} are the known physical coordinates of fibre nodes and X^{l}_{i} are the plate nodes.

In the current configuration, the kinematic relation is written as

$$Y^{f}_{i} = \phi_l(\xi^{P}_{1}, \xi^{P}_{2}) Y^{l}_{i} \tag{33}$$

where Y^{l}_{i} are the current positions of plate nodes. Equation (33) ensures the connection among nodes of fibres to the matrix.

4.3 General internal force

The strain energy stored in a reinforced body is the sum of the strain energy stored in the matrix and fibre, such as:

$$U = U_{mat} + U_{f} \tag{34}$$

where U_{mat} is the strain energy stored in the plate finite elements used to discretize the matrix and U_{f} is the strain energy stored in the fibre finite elements. Therefore, the internal force at a node β in the direction α of the plate element considering the contribution of the fibre is found by using the conjugate energy concept, such as:

$$\frac{\partial(U_{mat}+U_f)}{\partial Y_\alpha^\beta}=\frac{\partial U_{mat}}{\partial Y_\alpha^\beta}+\frac{\partial U_f}{\partial Y_\alpha^\beta}=\frac{\partial U_{mat}}{\partial Y_\alpha^\beta}+\frac{\partial U_f}{\partial Y_i^P}\frac{\partial Y_i^P}{\partial Y_\alpha^\beta}=F_\alpha^{\beta mat}+\phi_\beta(\xi_1^P,\xi_2^P)F_\alpha^{Pf}=F_\alpha^{\beta int} \quad (35)$$

where Equations (33) and (29) have been used and there is no summation over P.

4.4 Hessian Matrix

Proceeding in the same way as described for the calculation of internal forces, we develop the second derivative of strain energy of the reinforced finite element in relation to the plate nodal parameters, as follows

$$\frac{\partial^2 U}{\partial Y_\alpha^\beta \partial Y_\gamma^\xi}=\frac{\partial^2\left(U_{mat}+U_f\right)}{\partial Y_\alpha^\beta \partial Y_\gamma^\xi}=\int_{V_0}\frac{\partial^2(u_{mat}+u_f)}{\partial Y_\alpha^\beta \partial Y_\gamma^\xi}dV_0=\int_{V_0}\frac{\partial^2 u_{mat}}{\partial Y_\alpha^\beta \partial Y_\gamma^\xi}dV_0+\int_{V_0^f}\frac{\partial^2 u_f}{\partial Y_\alpha^\beta \partial Y_\gamma^\xi}dV_0^f \quad (36)$$

It is necessary to observe that the kernel of the last integral is the specific strain energy of a fibre derived twice regarding the plate nodal parameters and Equation (31) gives its value when derived regarding fibre parameters. So one has to apply twice the chain rule described by

$$\frac{\partial Y_i^P}{\partial Y_\alpha^\beta}=\frac{\partial Y_i^l}{\partial Y_\alpha^\beta}\phi_l(\xi_1^P,\xi_2^P)=\delta_{\alpha i}\delta_{\beta l}\phi_l(\xi_1^P,\xi_2^P)=\delta_{\alpha i}\phi_\beta(\xi_1^P,\xi_2^P) \quad (37)$$

that is $\partial Y_i^P/\partial Y_\alpha^\beta=\phi_\beta(\xi_1^P,\xi_2^P)$ if $\alpha=i$, over Equation (36), resulting

$$\begin{aligned}\frac{\partial^2 u_f}{\partial Y_\alpha^\beta \partial Y_\gamma^\xi}=&\frac{\partial^2 u_f}{\partial Y_\omega^{\rho f}\partial Y_w^{\rho f}}\frac{\partial Y_\omega^{\rho f}}{\partial Y_\alpha^\beta}\frac{\partial Y_\omega^{\rho f}}{\partial Y_\gamma^\xi}+\frac{\partial^2 u_f}{\partial Y_\omega^{\rho f}\partial Y_\pi^{\eta f}}\frac{\partial Y_\omega^{\rho f}}{\partial Y_\alpha^\beta}\frac{\partial Y_\pi^{\eta f}}{\partial Y_\gamma^\xi}+\frac{\partial^2 u_f}{\partial Y_\pi^{\eta f}\partial Y_\omega^{\rho f}}\frac{\partial Y_\pi^{\eta f}}{\partial Y_\alpha^\beta}\frac{\partial Y_\omega^{\rho f}}{\partial Y_\gamma^\xi}+\\&+\frac{\partial^2 u_f}{\partial Y_\pi^{\eta f}\partial Y_\pi^{\eta f}}\frac{\partial Y_\pi^{\eta f}}{\partial Y_\alpha^\beta}\frac{\partial Y_\pi^{\eta f}}{\partial Y_\gamma^\xi}\end{aligned} \quad (38)$$

or

$$\frac{\partial^2 u_f}{\partial Y_\alpha^\beta \partial Y_\gamma^\xi}=h^f_{\omega\rho\omega\rho}\frac{\partial Y_\omega^{\rho f}}{\partial Y_\alpha^\beta}\frac{\partial Y_\omega^{\rho f}}{\partial Y_\gamma^\xi}+h^f_{\omega\rho\pi\eta}\frac{\partial Y_\omega^{\rho f}}{\partial Y_\alpha^\beta}\frac{\partial Y_\pi^{\eta f}}{\partial Y_\gamma^\xi}+h^f_{\pi\eta\omega\rho}\frac{\partial Y_\pi^{\eta f}}{\partial Y_\alpha^\beta}\frac{\partial Y_\omega^{\rho f}}{\partial Y_\gamma^\xi}+h^f_{\pi\eta\pi\eta}\frac{\partial Y_\pi^{\eta f}}{\partial Y_\alpha^\beta}\frac{\partial Y_\pi^{\eta f}}{\partial Y_\gamma^\xi} \quad (39)$$

where h^f is the kernel of the fibre Hessian matrix described by Equation (31). In Equation (39) index notation is not adopted.

Integrating (39) over fibre volume gives:

$$\frac{\partial^2 U_f}{\partial Y_\alpha^\beta \partial Y_\gamma^\xi} = H^f_{\omega\rho\omega\rho} \frac{\partial Y_\omega^{\rho f}}{\partial Y_\alpha^\beta} \frac{\partial Y_\omega^{\rho f}}{\partial Y_\gamma^\xi} + H^f_{\omega\rho\pi\eta} \frac{\partial Y_\omega^{\rho f}}{\partial Y_\alpha^\beta} \frac{\partial Y_\pi^{\eta f}}{\partial Y_\gamma^\xi} + H^f_{\pi\eta\omega\rho} \frac{\partial Y_\pi^{\eta f}}{\partial Y_\alpha^\beta} \frac{\partial Y_\omega^{\rho f}}{\partial Y_\gamma^\xi} + H^f_{\pi\eta\pi\eta} \frac{\partial Y_\pi^{\eta f}}{\partial Y_\alpha^\beta} \frac{\partial Y_\pi^{\eta f}}{\partial Y_\gamma^\xi} \tag{40}$$

The resulting operation is the consistent spreading of fibres contribution over the matrix properties, represented by:

$$H = H_{ef} + H_f \tag{41}$$

4.5 Spreading operation for any order fibre

This item changes Equation (40) to a matrix form, simplifying the numerical application.

The Hessian matrix of the fibre $[H^f]_{2(GP^f+1)x2(GP^f+1)}$ is expanded into a matrix of order $(4(GP^f+1)Nx4(GP^f+1)N)$, by means of a sparse matrix $[\phi^\beta]_{2(GP^f+1)x4(GP^f+1)N}$, as:

$$\begin{aligned} H_f = \hat{H}_f &= [\hat{H}_f]_{4(GP^f+1)Nx4(GP^f+1)N} \\ &= [\phi^\beta]^T_{4(GP^f+1)Nx2(GP^f+1)} \cdot [H^f]_{2(GP^f+1)x2(GP^f+1)} \cdot [\phi^\beta]_{2(GP^f+1)x4(GP^f+1)N} \end{aligned} \tag{42}$$

where N is the number of nodes of the plate element, GP^f is the order of approximation of the fibre element and $[H^f]_{2(GP^f+1)x2(GP^f+1)}$ is obtained from Equation (31).

5 Numerical examples

In this section, we present the numerical examples simulated to shown the potential of our formulation.

5.1 Cantilever beam

This example compares the displacement result achieved by the proposed formulation and the one given by a general bar software Acadframe freely distributed at http://www.set.eesc.usp.br/portal/pt/softwares [12, 13] of a clamped reinforced beam subjected to a uniform distributed load, see Figure 3.

The adopted geometrical properties are: $L = 300cm$, $h = 10cm$, $b = 1cm$, $d = 2,5cm$ and $h' = 7,5cm$. The transverse applied load is $q = 50N/cm$. The Young modulus and the Poisson´s ratio of the matrix are $E_c = 21x10^5\ N/cm^2$ and $\nu = 0$,

while the Young modulus and the cross-sectional area of the fibre are $E_f = 210x10^5\ N/cm^2$ and $A_f = 0,1cm^2$.

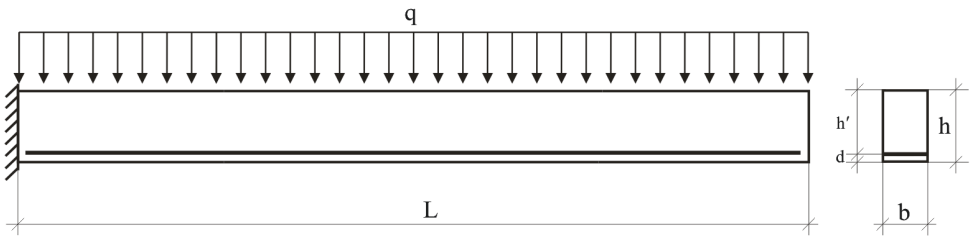

Figure 3: Cantilever beam.

When using the proposed reinforcement procedure the matrix is discretized by 300 quadratic plate elements totalizing 671 nodes and 1342 degrees of freedom and the reinforcement is discretized by 120 linear and 60 quadratic fibre elements. The analysis made by Acadframe applies 10 bar elements of 5th order following the Thimoshenko-Reissner kinematics. The analysis is performed in 10 load steps. The achieved result for the proposed formulation is depicted in Figure 4.

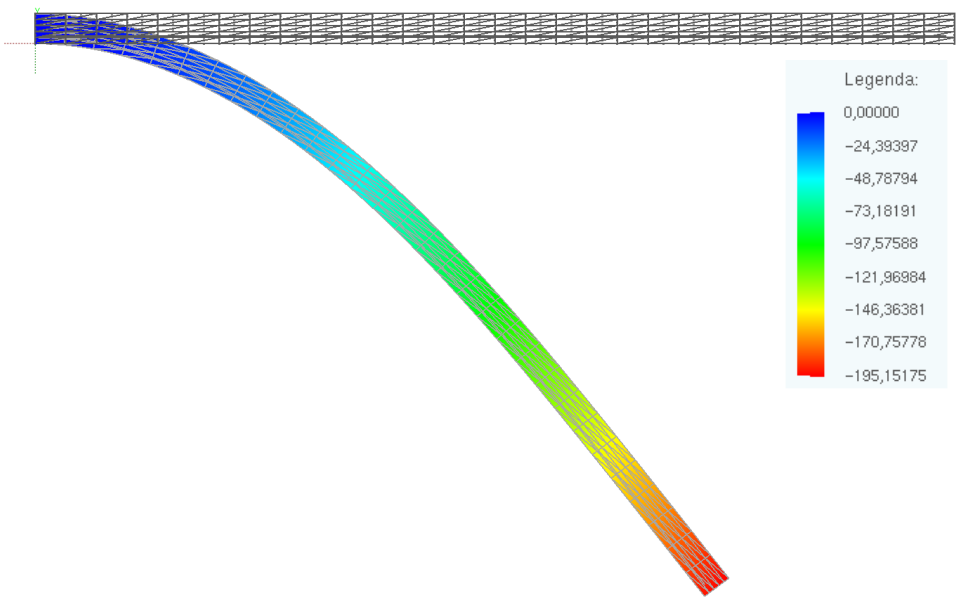

Figure 4: Deformed configuration in (cm) of the cantilever beam.

Comparing the maximum deflection in the central node of the free end of the cantilever beam obtained with the proposed formulation, $\delta \cong 187,263cm$, with the corresponding result of the AcadFrame, $\delta \cong 183,168cm$, there is a relative difference of $2,235\%$, showing the consistency of the proposed method. Obviously the solid solution is larger than the general bar solution, as less kinematical restrictions are made.

Moreover, it is possible to observe that the mechanical coupling between fibre and matrix is properly working.

5.2 Conform coupling between fibre and matrix

This item uses the analysis of some hypothetical plates to demonstrate the total adhesion between fibre and matrix when the approximation order of fibres is higher or equal to the plate element order.

Three analyses of a triangular plate are carried out. The first analysis adopts a single linear plate element reinforced by a vertical fibre. The fibre is modelled by three different approximation orders, from linear to third order. The other two analysis are similar, however the element order is increased from the linear to the third order plate element.

The Young modulus and the Poisson´s ratio of the matrix are $E_c = 1\,N/cm^2$ and $\nu = 0$, while the Young modulus and the cross-sectional area of the fibre are $E_f = 0\,N/cm^2$ and $A_f = 0,1cm^2$ for all cases. The lower points are totally constrained and a horizontal force of $F = 5N$ is applied on the top node. The triangle side is $L_c = 200cm$ and the fibre length is $L_f = 170cm$ distant $10cm$ from the base.

The objective of the analysis is to verify whether points along the fibre (different from nodes) present relative movement regarding the continuum points after a change of configuration. It is done by choosing the fibre dimensionless coordinates of the analyzed points, in this case 12 equally spaced points. By means of fibre shape functions we determine the physical coordinates of these points at initial configuration. With these physical coordinates we determine the corresponding plate dimensionless coordinates, Equation 50. After applying the external force and finding the equilibrium nodal position, using the fibre shape functions we determine the current positions of that 12 fibre points. With the plate shape functions we determine the corresponding continuum current positions of the same points. In proper tables we compare these values for which when they are different occurs relative movement, when not, total adhesion is guaranteed.

The plate and fibres discretizations for the first analysis (linear plate element) and for the second analysis (second order plate approximation) are shows in the first line of the Figure 5 and Figure 6, respectively. The second line illustrates the horizontal displacements and the third line illustrates the vertical displacements. One observes that the plate approximation, in the first case, is always linear, and in the second case is always quadratic. The fibre approximation grows from left to right.

It is possible to infer from Figure 5 that there is no relative displacement between fibre and continuum points for any adopted fibre order.

Similarly, it is possible to infer from Figure 6 that there is relative displacement between the linear fibre and continuum points, however for quadratic (or over) fibre approximation there is no relative movement.

The first line of Figure 7 shows the plate and fibres discretizations for the third analysis (cubic plate element), the second line illustrates the horizontal displacements and the third line illustrates the vertical displacements. One observes that the plate approximation is always cubic, while the fibre approximation grows from left to right.

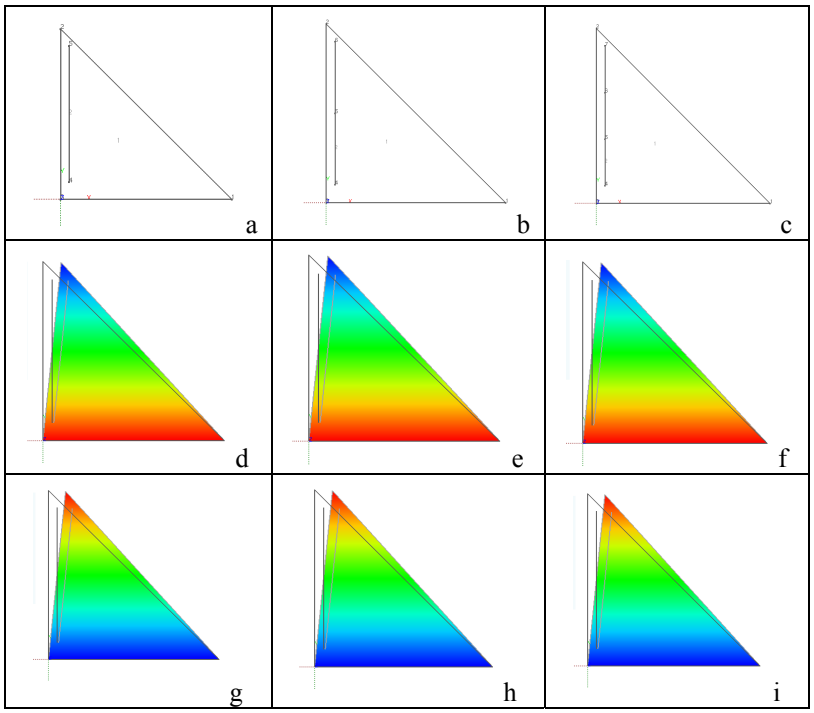

Figure 5: Linear two-dimensional plate element.

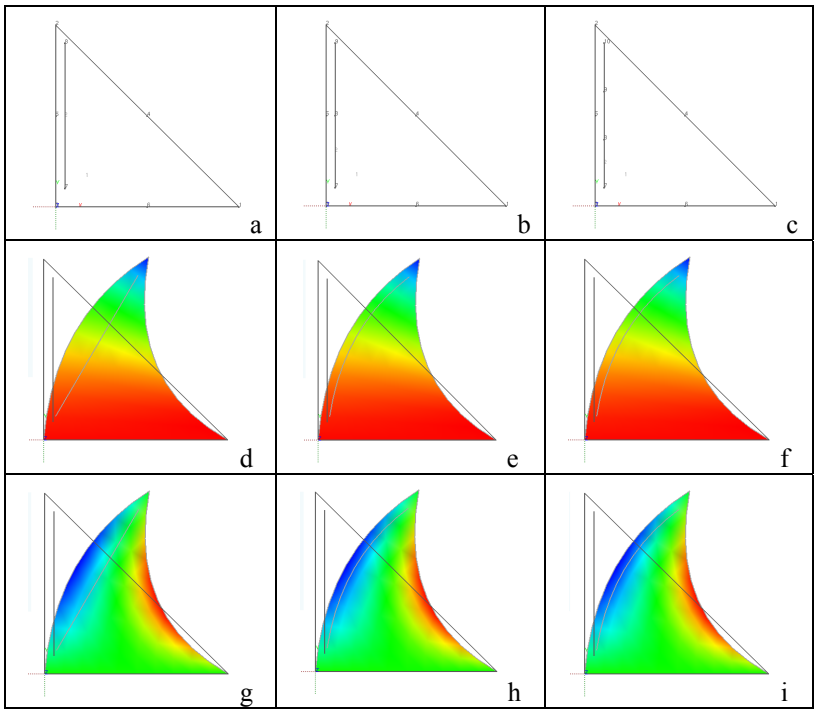

Figure 6: Quadratic two-dimensional plate element.

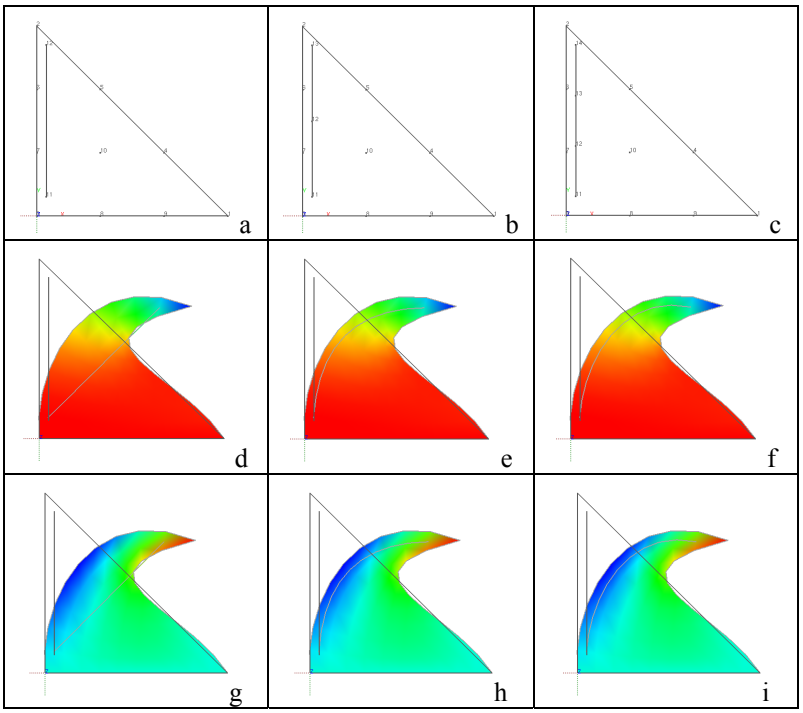

Figure 7: Cubic two-dimensional plate element.

It is possible to infer from Figure 7 that there is relative displacement between the linear and quadratic approximations of fibre and continuum points, however for cubic fibre approximation there is no relative movement. This behavior is proved numerically in Table 1 in which the current positions of fibre and continuum points are compared to each other.

DEGREE OF FREEDOM	POSITIONS					
	SOLID: 3º	FIBER: 1º	SOLID: 3º	FIBER: 2º	SOLID: 3º	FIBER: 3º
1	9,7266664353850	9,7266664353850	9,7266664353850	9,7266664353850	9,7266664353850	9,7266664353850
2	23,3324281933738	23,3324281933738	23,3324281933738	23,3324281933738	23,3324281933738	23,3324281933738
3	11,7813907434346	20,6586943438326	11,7813907434346	12,0036556098185	11,7813907434346	11,7813907434346
4	40,9811551578689	34,4645510662076	40,9811551578689	44,3915004212943	40,9811551578689	40,9811551578689
5	15,7004817181174	31,5907222522803	15,7004817181174	16,0116525310549	15,7004817181174	15,7004817181175
6	58,6906994094019	45,5966739390414	58,6906994094019	63,4651827781974	58,6906994094019	58,6906994094020
7	21,4543040439156	42,5227501607279	21,4543040439156	21,7506571990941	21,4543040439156	21,4543040439156
8	76,0063482461828	56,7287968118751	76,0063482461828	80,5534752640831	76,0063482461827	76,0063482461828
9	29,0132224053111	53,4547780691756	29,0132224053111	29,2206696139361	29,0132224053111	29,0132224053112
10	92,4733889664213	67,8609196847089	92,4733889664213	95,6563778789516	92,4733889664213	92,4733889664213
11	38,3476014867864	64,3868059776232	38,3476014867864	38,4216897755809	38,3476014867864	38,3476014867863
12	107,6371088683280	78,9930425575427	107,6371088683280	108,7738906228030	107,6371088683280	107,6371088683280
13	49,4278059728232	75,3188338860708	49,4278059728232	49,3537176840286	49,4278059728232	49,4278059728232
14	121,0427952501120	90,1251654303765	121,0427952501120	119,9060134956360	121,0427952501120	121,0427952501120
15	62,2242005479040	86,2508617945185	62,2242005479040	62,0167533392790	62,2242005479040	62,2242005479040
16	132,2357354099830	101,2572883032100	132,2357354099830	129,0527464974530	132,2357354099830	132,2357354099830
17	76,7071498965109	97,1828897029662	76,7071498965109	76,4107967413323	76,7071498965108	76,7071498965109
18	140,7612166461520	112,3894111760440	140,7612166461520	136,2140896282520	140,7612166461520	140,7612166461520
19	92,8470187031259	108,1149176114140	92,8470187031259	92,5358478901884	92,8470187031259	92,8470187031259
20	146,1645262568290	123,5215340488780	146,1645262568290	141,3900428880340	146,1645262568290	146,1645262568290
21	110,6141716522310	119,0469455198610	110,6141716522310	110,3919067858470	110,6141716522310	110,6141716522310
22	147,9909515402230	134,6536569217120	147,9909515402230	144,5806062767980	147,9909515402230	147,9909515402240
23	129,9789734283090	129,9789734283090	129,9789734283090	129,9789734283090	129,9789734283090	129,9789734283090
24	145,7857797945450	145,7857797945450	145,7857797945450	145,7857797945450	145,7857797945450	145,7857797945450

Table 1: Nodal positions of the cubic two-dimensional plate element.

As one can observe the conform coupling between fibre-matrix is guaranteed if the fibre approximation order at least the same as the plate element order.

6 Conclusions

A curved fibre finite element with high order approximations based on a tailoring description is developed in this paper. The use of fibre elements with equal or higher order of approximation to the continuum approximation ensures the conform coupling between the fibre and the matrix. The numerical examples show the generality and accuracy of the proposed formulation. Future works on the subject should comprise the interface stress components calculations.

Acknowledgements

This research is supported by CAPES (Brazil), Amazonas Research Foundation (FAPEAM) and São Paulo Research Foundation (FAPESP).

References

[1] F.K.F. Radtke, A. Simone, L.J. Sluys, “A partition of unity finite element method for simulating non-linear debonding and matrix failure in thin fiber composites”, International Journal for Numerical Methods in Engineering, 86(4-5), 453-476, 2011.

[2] F.K.F. Radtke, A. Simone, L.J. Sluys, “A partition of unity finite element method for obtaining elastic properties of continua with embedded thin fibres”, International Journal for Numerical Methods in Engineering, 84(6), 708-732 , 2010.

[3] F.K.F. Radtke, A. Simone, L.J. Sluys., “A computational model for failure analysis of fibre reinforced concrete with discrete treatment of fibres”, Engineering Fracture Mechanics, 77(4), 597-620, 2010.

[4] L. Vanalli, R.R. Paccola, H.B. Coda, “A simple way to introduce fibers into FEM models”, Communication in numerical methods in Engineering, 24, 585-603, 2008.

[5] P.G. Ciarlet, “Mathematical Elasticity”. North-Holland, 1993.

[6] R.W. Ogden, “Non-linear Elastic deformation”, Ellis Horwood, England, 1984.

[7] T.R. Tauchert, “Energy principles in structural mechanics”, McGraw Hill, 1974.

[8] Luenberger, D. G. “Linear and nonlinear programming”. Addison-Wesley Publishing Company, 1989.

[9] J. Bonet J, R.D. Wood, J. Mahaney, P. Heywood, "Finite element analysis of air supported membrane structures", Computer Methods in Applied Mechanics and Engineering, 190(5-7), 579-595, 2000.

[10] H.B. Coda, R.R. Paccola, “An alternative positional FEM formulation for geometrically non-linear analysis of shells: Curved triangular isoparametric elements”, Computational Mechanics, 40(1), 185-200, 2007.
[11] L. Vanalli, “O MEC e o MEF aplicados à análise de problemas viscopásticos em meios anisotrópicos e compostos”. Ph.D. Thesis, SET, University of São Paulo, São Carlos, Brazil, 2004.
[12] H.B. Coda; M. Greco, “A simple FEM formulation for large deflection 2D frame analysis based on position description”, Computer Methods in Applied Mechanics and Engineering, 193(33-35), 3541-3557, 2004.
[13] H.B. Coda; R.R. Paccola, “Improved finite element for 3D laminate frame analysis including warping for any cross-section”, Applied Mathematical Modelling, 34(4), 1107-1137, 2010.